HYDROGEN FUEL CELL & ENERGY STORAGE

Metal-organic framework-derived Cu@Co_4N nanoparticles anchored on N-doped carbon nanotubes for efficient and stable ORR activity

Parisa Akbarian[a] | **Mehdi Kheirmand**[a, b,*]

a Hydrogen and Fuel Cell Research Laboratory, Department of Chemistry, Yasouj University, Yasouj, Iran
b Department of Chemistry, School of Basic Sciences, Yasouj University, PO Box 75918-74934, Yasouj, Iran
* Corresponding Author's E-mail Address: Kheirmand@yu.ac.ir

Article Information

Article Type:
Research Article

Article History:

Received: 19 August 2023
Received in revised form 29 November 2023
Accepted: 20 Dec 2023
Published on line 25 December 2023

Keywords

Oxygen Reduction Reaction, electrocatalyst
Metal-Air Battery
M-N-C Catalysts
Metal-Organic Frameworks

Abstract

Developing highly efficient, durable, and low-cost electrocatalysts for the oxygen reduction reaction (ORR) is very important for energy conversion technologies. Electrocatalysts with porous structures, numerous active sites, and earth-abundant are exceedingly favorable for ORR reaction. In this work, the 3D nano hollow-shell Cu@Co_4N anchored on N-doped carbon nanotubes (Cu@Co-N-C) was synthesized using pyrolyzed Cu@ZnCoZIF. The synthesized Cu@Co-N-C with bimetallic active sites, high specific surface area, high porosity structure, and nitrogen doping level demonstrated superior ORR activity. The physical characteristics of the cathode electrocatalysts were assessed through X-ray powder diffraction (XRD), scanning electron microscopy (FESEM), transmission electron microscopy (TEM), Brunauer-Emmett-Teller (BET), Raman, and energy dispersive X-ray analysis (EDX) for elemental mapping. The electrocatalyst illustrated a higher half-wave potential of 0.88 V vs. RHE than that of the Pt/C electrocatalyst in an alkaline electrolyte. Moreover, it also has excellent ORR stability, making it one of the best Pt-free electrocatalysts. The current density of the Cu@Co-N-C is approximately -5.46 mA cm^{-2}, which is higher than that of Co-N-C (-4.20 mA cm^{-2}) and NCNTs (-1.9 mA cm^{-2}). Moreover, higher stability was obtained for Cu@Co-N-C in comparison with Pt/C. So, this material is an excellent choice as a cathodic catalyst for application in metal-air fuel cells.

Cite this article: Akbarian, P., Kheirmand, M (2023). Metal-organic framework-derived Cu@Co_4N nanoparticles anchored on N-doped carbon nanotubes for efficient and stable ORR activity. DOI:10.22104/HFE.2023.6585.1273

Publisher:Iranian Research Organization for Science and Technology(IROST)
DOI:10.22104/HFE.2023.6585.1273

1. Introduction

The oxygen reduction reaction (ORR) is a substantial electrochemical process for progressed energy storage and conversion systems (such as metal-air batteries and fuel cells) to solve the ever-increasing use of fossil energy and accompanying vigorous environmental issues [1-3]. The ORR is a critical reaction in these systems that occurs in the cathode [4, 5]. Because of the sluggish kinetics of the ORR, many catalysts have been studied to facilitate this reaction. Since platinum has high activity as the catalyst, it has been extensively investigated [6-8], and although Pt has been the best catalyst for the ORR for a long time, it has a high cost and is not commodious [9]. For this purpose, other more available, cheaper, and environmentally friendlier catalysts than platinum for the ORR, such as metal oxides, metal carbides, metal nitrides, Pt-alloy, spinel, and organometallic, have been investigated [10-15]. A catalyst's performance and catalytic activity are influenced by the morphology, size, and ratio of metals, making these features important for their effectiveness [16]. Metal and nitrogen-codoped on carbon support (M-N-C) catalysts, such as Pt-based electrocatalysts, have been considered the most promising candidates to replace precious electrocatalysts. Fe-N-C and Co-N-C have been indicated to have excellent ORR activity in both acidic and alkaline electrolytes [17, 18].

Metal–organic frameworks (MOFs), which contain metal ions/cluster centers and organic bridging ligands, have favorable characteristics, such as suitable porosity size, versatile surface geometry, high specific surface area, N species, and tunable metals and ligands and exhibit significant electrical conductivity and long-term durability. Zeolitic imidazolate frameworks (ZIFs), a subclass of MOFs, have appeared as a new structure for producing M-N-C electrocatalysts. Furthermore, the compound of the M-N-C structures can be determined by changing metals or ligands, and ZIFs display remarkable durability in alkaline electrolytes. Notably, metal doping over ZIFs can modify their microstructure, bandgap structure, and electrical conductivity properties [19-21]. Cu is a promising transition metal with outstanding ORR activity because its position is near Pt at the top of the "volcano plot." However, inevitable aggregation and surface oxidation take place when Cu-based carbon materials are generated via pyrolysis, which restricts their electrocatalytic efficiencies [22, 23]. Moreover, the synergistic effects among bimetallic or trimetallic active sites have been evidenced to further enhance the ORR activity because the alteration of surface charge distribution of active sites leads to improved charge transfer and decreases the energy barrier in the activation of ORR [24].

In this work, we developed a superior ORR electrocatalyst with a 3D hollow-shell structure of Cu@Co-N-C using pyrolysis of Cu-ZnCoZIF. The abundant pores, large surface area, and highly dispersed and exposed active sites improve the ORR activity of Cu@Co-N-C. The as-synthesized Cu@Co-N-C nanohybrid exhibited extraordinary ORR activity with an excellent half-wave potential ($E_{1/2}$) of 0.88 V vs. RHE and greater stability than commercial Pt/C.

2. Experimental

2.1. Chemicals and Materials

Zinc nitrate hexahydrate (AR), Cobalt nitrate hexahydrate (AR), Copper nitrate trihydrate (AR), Potassium hydroxide (95%), Urea, Methanol, and Ethanol were purchased from the Merck Company. 2-methylimidazole was purchased from Alfa Aesar. Nafion solution (D520, 5%) was obtained from Dupont, and Pt/C (20 wt % of Pt) and RuO_2 were purchased from Sigma-Aldrich.

1.2. Synthesis of Cu@Co-N-C electrocatalyst

1.2.1. Synthesis of graphitic carbon nitride (g-C_3N_4)

Firstly, the g-C_3N_4 was prepared using the previously reported method with minor modifications [25]. In brief, urea (7 g) was ground in an agent mortar, transferred into an alumina boat crucible, and then placed in a tube furnace. The sample was annealed to 550 ℃ with a heating rate of 5 °C min^{-1}, preserved at 550 °C for 2 h under a flowing argon atmosphere, and then naturally cooled to ambient temperature. Finally, the g-C_3N_4 was successfully prepared.

1.2.2. Synthesis of Cu@Co-N-C

To achieve Cu-ZnCoZIF, g-C_3N_4 (0.05 g) was dissolved in 40 mL methanol containing $Zn(NO_3)_3.6H_2O$ (0.22 g), $Co(NO_3)_2.6H_2O$ (0.058 g (2×10^{-4})), and $Cu(NO_3)_3.3H_2O$ (0.019 g (1×10^{-4})), then sonicated for 1 h. Afterward, 2-methylimidazole (0.86 g) was dissolved in the sonicated blend by stirring at 35 ℃ for 4 h; then, the crystals were collected by centrifugation and washed with methanol several times and dried in a vacuum oven at 60 ℃ overnight. Finally, to obtain a 3D hollow-nano shell, Cu@Co-N-C **(**the Cu-ZnCo-ZIF) was placed in a tube furnace and pyrolyzed under a nitrogen atmosphere at a heating rate of 5 ℃ min^{-1} and 930 ℃ for 2 h, then naturally cooled to ambient temperature under nitrogen atmosphere. For comparison, a series of control samples of N-doped carbon nano-dodecahedra/N-doped carbon nanotubes (NC/NC) (without $Co(NO_3)_2.6H_2O$ and $Cu(NO_3)_3.3H_2O$) and Co-N-C were also constructed through the same method.

1.3. Materials characterization

The crystallinity of the samples was identified by X-ray powder diffraction (XRD; model Philips PW1730). The detailed morphologies and structures of samples were characterized by transmission electron microscopy (TEM; model Philips EM 208S) and field emission scanning electron microscopy (FESEM; model TESCAN MIRA3). Elemental mapping and energy dispersive spectrometer (EDS) were also analyzed by TESCAN MIRA3. Specific surface areas of the obtained carbon materials and pore size distribution of samples were recorded by Brunauer-Emmett-Teller (BET; model Belsorp mini II from Microtrac Bel Corp Co.). The Raman spectra were assembled by UniDRON-UniNanoTech Raman spectroscopy.

1.4. Electrochemical measurements

ORR electrochemical performances were performed in a conventional three-electrode cell on an EG&G potentiostat/galvanostat (PARStAT 2273) instrument. The counter electrode was Pt sheet, the reference electrode was Hg/HgO (saturated KCl), and the working electrode was prepared as follows: 3 mg catalyst were ultrasonically dispersed into the mixture of deionized water:ethanol:nafion (0.5 mL:0.5 mL:0.03 mL) for 30 min to form a homogeneous catalyst ink. Eight µL of ink catalyst was dropped onto a glassy carbon rotating disk electrode. The active area of the electrode was 5 mm, and the catalyst loading was 0.3 mg cm^{-2}. For comparison, commercial Pt/C (20 wt%) catalysts were prepared using the same method as a working electrode. Fresh KOH (0.1 M) saturated with O_2 for 30 min was applied as an electrolyte for all electrochemical tests in this study. All values of the potentials were converted to reversible hydrogen electrode (RHE) according to the equation: $E_{(RHE)} = E_{(MOE)} + \varphi_{(MOE)} + 0.059 * pHV$ [1]. Linear sweep voltammetry (LSV) was performed at a scan rate of 10 mV s^{-1} under various rotating speeds (400 rpm, 625 rpm, 900 rpm, 1225 rpm, 1600 rpm, 2025 rpm, and 2500 rpm) from 0.2 to 1.2 V *vs.* RHE, respectively. The Koutecky-Levich equation, as shown below, was used to evaluate the transferred electron number (n) per O_2 molecule in the ORR process under different

potentials [26].

$$j^{-1} = j_K^{-1} + j_L^{-1} = j_k^{-1} + \left(B_\omega^{-1/2}\right)^{-1} \quad (1)$$

$$B = 0.62nFAC_o D_o^{2/3} \upsilon^{-1/6} \quad (2)$$

where j is the measured current density, j_k is the kinetic current density, ω is the rotation rate of the electrode, n is the electron transfer number, C_{O2} is the bulk concentration of O_2 (1.2×10^{-3} mol L^{-1} for 0.1 M KOH solution), F is the Faraday constant (96485 C mol^{-1}), Do_2 is the diffusion coefficient of O_2 (1.9×10^{-5} cm^2 s^{-1} for 0.1 M KOH solution), and υ is the kinetic viscosity (0.01 cm^2 s^{-1} for 0.1 M KOH solution).

The durability of the electrocatalyst for ORR was measured by LSV in the potential range of 0.2 to 1.2 V *vs.* RHE at 100 mV s^{-1} for 6000 cycles. Chronoamperometry (CA) was performed to investigate the stability of the electrocatalyst at 0.75 V for 7000 s and then compared to the stability of the Pt/C 20%wt. Electrochemical impedance spectroscopy (EIS) measurement of the electrocatalyst was carried out at a frequency range of 100 kHz- 1 mHz with an applied voltage of 0.75 V *vs.* RHE.

3. Results and discussion

The morphologies of the as-synthesized Cu@Co-N-C were studied by FESEM and TEM. As can be seen in Fig. 1a, the hollow-shell polyhedral structure of Cu@Co-N-C with a diameter size of about 154 nm for Cu@Co-N-C and 35 nm for NCNTs is well-formed by carbonization at 930 °C to evaporate zinc metal and preserved the hollow structure with NC shells to prevent the aggregation of Cu and Co [27]. The decomposition of g-C_3N_4 and zinc metal provides N-doped carbon nanotubes and NC shells that surround Cu@Co_4N, enhancing the durability and resistance of Cu@Co-N-C toward corrosion and other environmental factors [28]. In addition, the porous structure is well-defined in FESEM.

The TEM image of Cu@Co-N-C, depicted in Fig. 1b, disclosed porous polyhedron nano-species shapes scattered homogeneously on NCNTs without any large agglomeration. At 930 °C, the zinc particles are completely evaporated. The Cu and Co metals are well scattered in the holes with the NC shell due to the evaporation of Zn, which hampers the agglomeration of metals on the surface. Excellent electrocatalytic activity and stability are achieved due to the strong interaction and synergistic effects between the graphitic carbon layers and Cu@Co_4N nanoparticles [29]. The elemental mapping image (Fig. 1c) illustrates that Cu, Co, N, and C are uniformly dispersed over the electrocatalyst.

X-ray diffraction (XRD) was then performed to investigate the structure of Cu@Co-N-C. Fig. 2a indicated a broad peak around 26.5°, assigned to the (002) plane of the graphitic carbon. The three peaks at 44, 51.5, and 76 are ascribed to the (111), (200), and (220) plans of Co_4N (JCPDF No. 150806), without any other peaks belonging to Cu, proving that Cu partially replaced the Co sites in the Co nano-species. The peaks at 44.5 and 65 in Cu@Co-N-C confirm the well-manufactured bimetallic CuCo. The EDX analysis result of the as-synthesized electrocatalyst is displayed in Fig. 2b. It exhibits peaks in the specific energy values related to Co, Cu, N, and C elements. Raman spectroscopy of Cu@Co-N-C is shown in Fig. 2c. There are two prominent peaks at 1344 cm^{-1} (band D) and 1581 cm^{-1} (band G) for Cu@Co-N-C. Additionally, the 2D peaks of the electrocatalyst can be identified at 2746.64 cm^{-1}, which confirms the formation of multi-layer graphitic films in the porous carbon substances [30]. The thicker graphitic structure represents more edges and defects, which are excellent for N doping. Besides, a thicker structure would be more durable and more resistant to corrosion than a thinner structure. The broad 2D peak with a lower intensity of Cu@Co-N-C than NC/NC demonstrates the formation of thick multi-layer graphene that is more

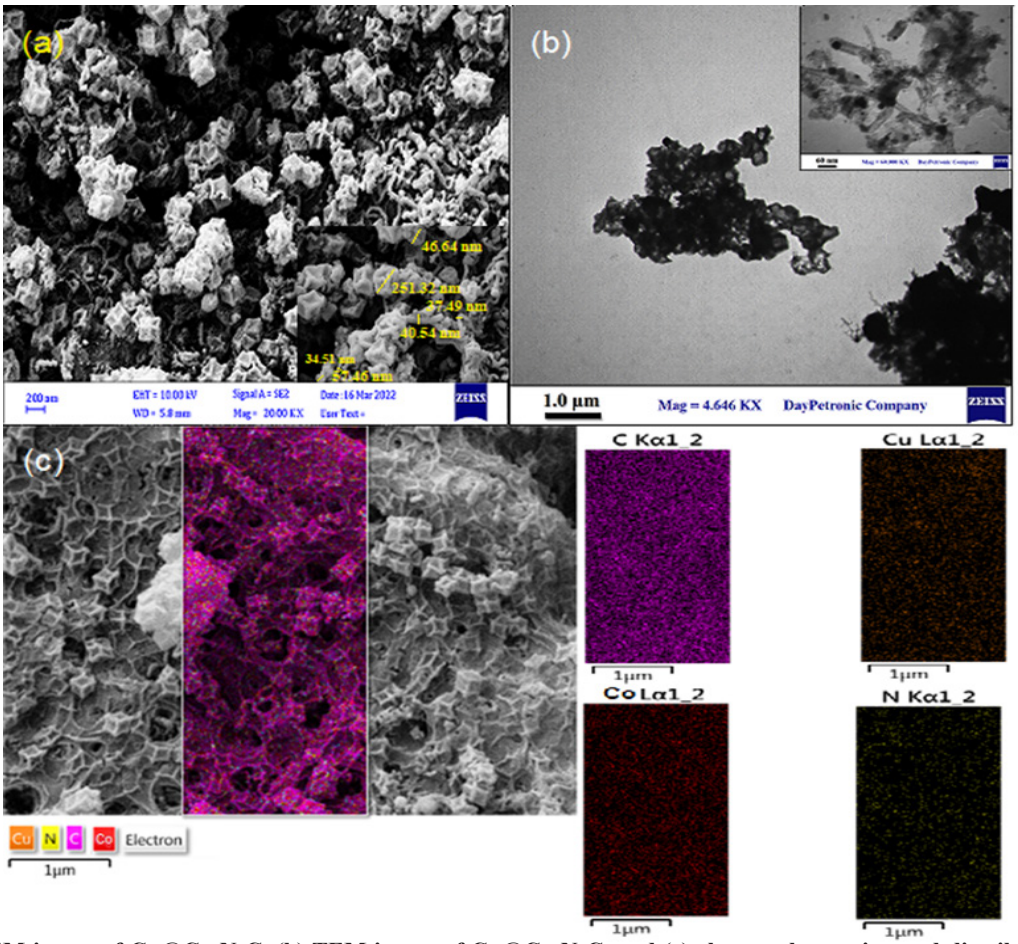

Fig. 1. (a) FESEM image of Cu@Co-N-C, (b) TEM image of Cu@Co-N-C, and (c) elemental mapping and distribution of Cu@Co-N-C.

stable and more resistant to corrosion.

The value of $I_D/I_G = 0.91$ for Cu@Co-N-C is lower than that of pure NC/NC (1.02), but both the peak intensities of the D and G bands of Cu@Co-N-C are more intense than that of NCNDs@NCNTs (NC@NC), confirming a high graphitization degree with abundant defect sites due to the incorporation of heterogenous atoms (Cu, Co and N) and the formation of more CNTs in the sample. The specific pore surface areas of Cu@Co-N-C were characterized by N_2 adsorption-desorption curves (Fig. 2d). The IV isotherm shape represents mesoporous materials for Cu@Co-N-C with an average pore size of 423.25 m^2g^{-1} using the Brunauer-Emmett–Teller. As a result, the 3D nano hollow-shell structure with a high specific surface area leads to superior electrocatalytic activity.

As can be seen in Fig. 3a, the Cu@Co-N-C has superior ORR activity compared to other catalysts. The onset and half-wave potential ($E_{1/2}$) of Cu@Co-N-C are 1.02 V and 0.88 V *vs.* RHE, which is higher than other electrocatalysts and even commercial Pt/C (TABLE I).

Table 1. The electrocatalytic performances of various electrocatalysts and Pt/C for oxygen reduction reaction in 0.1 M O_2-saturated KOH electrolyte.

catalysts	Electrochemical measurements		
	Eonset (V vs. RHE)	$E_{1/2}$ (V vs. RHE)	Current density (mA.cm^{-2})
Pt/C	0.99	0.81	-5.47
Cu@Co-N-C	1.02	0.88	-5.46
Co-N-C	1.01	0.79	-4.20
NC@NC	0.88	0.66	-1.9

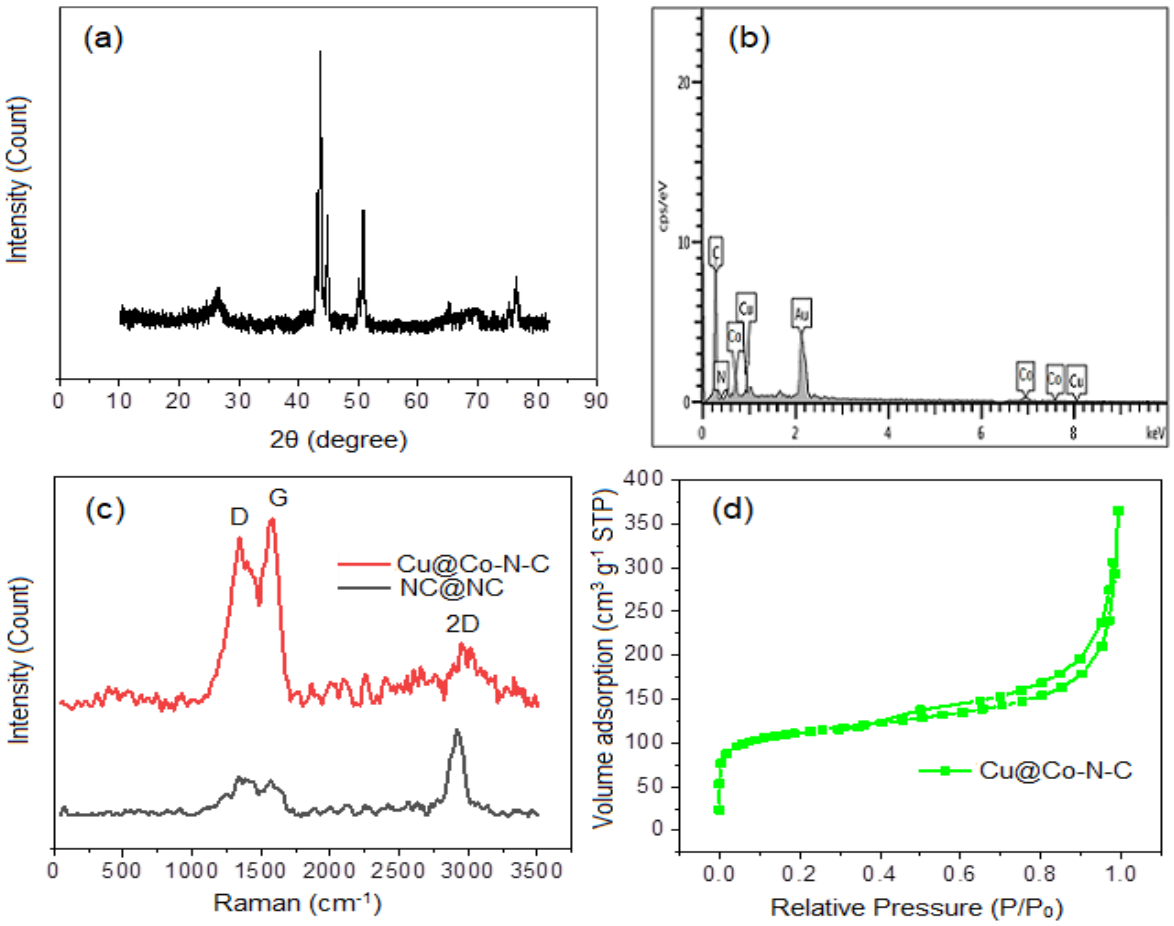

Fig. 2. (a) XRD patterns of Cu@Co-N-C, (b) EDX pattern of the Cu@Co-N-C electrocatalyst, (c) Raman spectra of Cu@Co-N-C and NC@NC, and (d) N_2 adsorption-desorption isotherms of Cu@Co-N-C.d

These results confirm the strong synergistic effects among nanoparticles such as Cu and Co that lead to high charge transfer and increasing ORR activity. For more knowledge into the ORR mechanism of Cu@Co-N-C electrocatalyst, LSVs at various rotating rates (400-2500 rpm) at a scan rate of 10 mVs^{-1} are obtained, as shown in Fig. 3b. Increasing the rotation rate also increased the limiting current density, confirming mass transfer is controlled by diffusion phenomenon. The Koutecky-Levich (K-L) plot derived from the LSVs curve is shown in Fig. 3c. The numbers of transferred electrons (n) from K-L slopes were calculated as 3.88, exhibiting a direct 4-electron reduction mechanism for the Cu@Co-N-C electrocatalyst. As a result, we can conclude that Cu@Co-N-C is an efficient ORR catalyst with a low peroxide (HO_2^-) product through the ORR process. To better study the accuracy of the ORR kinetics, the Tafel curves of the electrocatalysts derived from LSVs are displayed in Fig. 3d. A lower Tafel slope confirms better kinetics for the ORR. The Tafel slope of Cu@Co-N-C is 49.6 mV dec^{-1}, which is very close to Pt/C (46.7 mV dec^{-1}) and much lower than other catalysts, demonstrating extraordinary ORR kinetics for Cu@Co-N-C.

The stability of Cu@Co-N-C and Pt/C was assessed using LSV in a 0.1M KOH electrolyte for 6000 cycles in ORR processes. The first and 6000th cycles of the corresponding LSV curves are illustrated in Fig. 4a, b. After 6000 cycles, the half-wave potential of Cu@Co-N-C was only enhanced by 3 mV, whereas this value was enhanced to 32 mV for Pt/C.

In addition, the stability of the Cu@Co-N-C and the

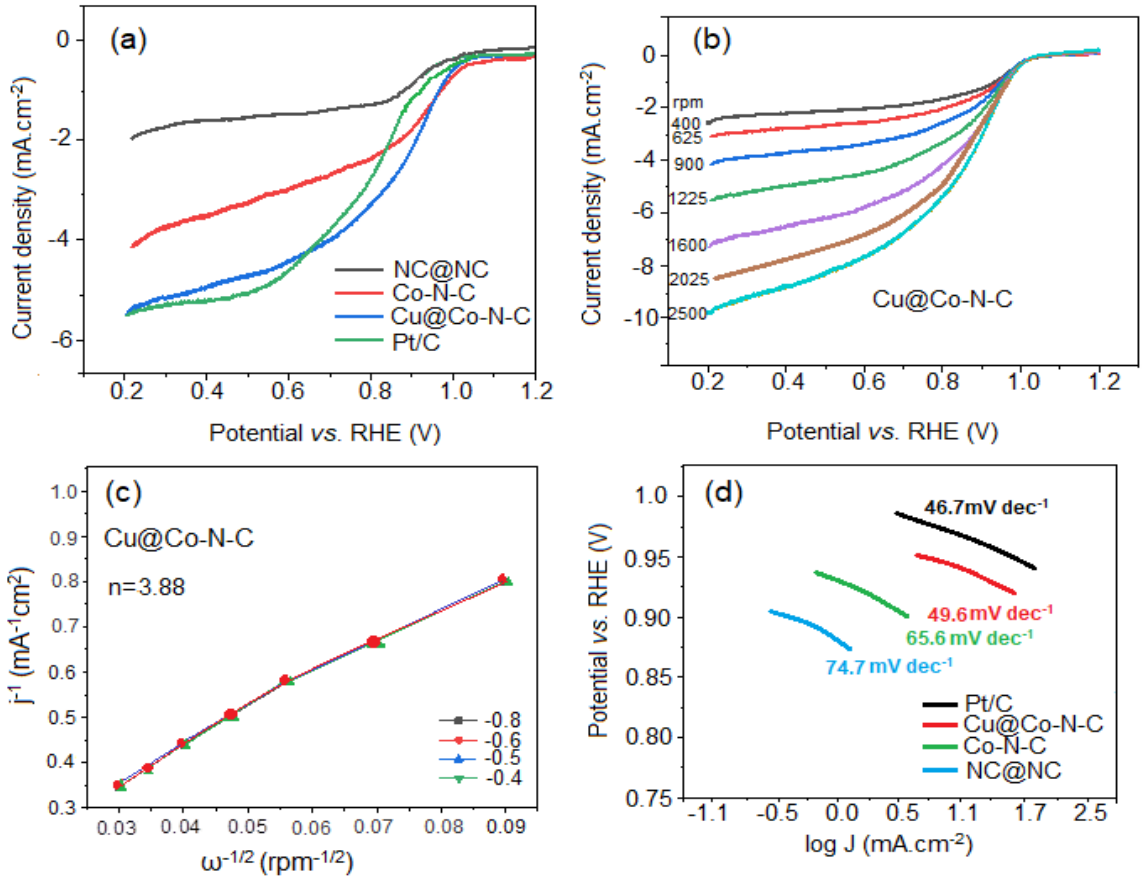

Fig. 3. (a) LSVs of Cu@Co-N-C, Co-N-C, NC@NC, and Pt/C at a rotating speed of 1600 rpm with a scanning speed of 10 mV s^{-1}. (b) LSVs of Cu@Co-N-C at various rotating rates of 400–2500 rpm with a scanning speed of 10 mV s^{-1}; (c) K–L plots at -0.4 to -0.8 V of Cu@Co-N-C, and (d) Tafel slopes of all as-prepared samples.

commercial Pt/C is illustrated in Fig. 4c using Chronoamperometric analysis at 0.75 V for 7000 s. The current density of Cu@Co-N-C holds at 91.3%, while the current density of Pt/C remains steady at 72.5% after 7000 s. The chronoamperometric test exhibits that the Cu@Co-N-C electrocatalyst holds greater stability than that of commercial Pt/C. The remarkable stability of Cu@Co-N-C is due to the porous and conductive structure of the 3D nano hollow-shell structure of $Cu@Co_4N$ on NCNTs.

Moreover, electrochemical impedance spectroscopy (EIS) of as-synthesized Cu@Co-N-C and Pt/C electrocatalysts was obtained to further analyze catalytic activity and electrode kinetics at 0.75 V *vs.* RHE in 0.1 M KOH from 10 kHz to 1 mHz and Nyquist plots. The corresponding circuit fitting plot are illustrated in Fig. 4d. The X-axis intercept in the high-frequency region illustrates the resistance of the solution (Rs). In contrast, the radius of the semicircle is related to the charge transfer resistance (R_{ct}) of the electrolyte interface/electrode material [31]. The R_{ct} for Cu@Co-N-C (5.26 Ω) is smaller than Pt/C (7.56 Ω), demonstrating a much faster reaction rate and higher electrical conductivity for Cu@Co-N-C.

Conclusion

In summary, a Cu-ZnCoZIF derived Cu@Co-N-C electrocatalyst was synthesized using the facile method for ORR. Due to bimetallic active sites, high N doping, and a mesoporous hierarchical structure with a high specific surface area of 423.25 m^2 g^{-1}, the as-synthesized Cu@Co-N-C contained

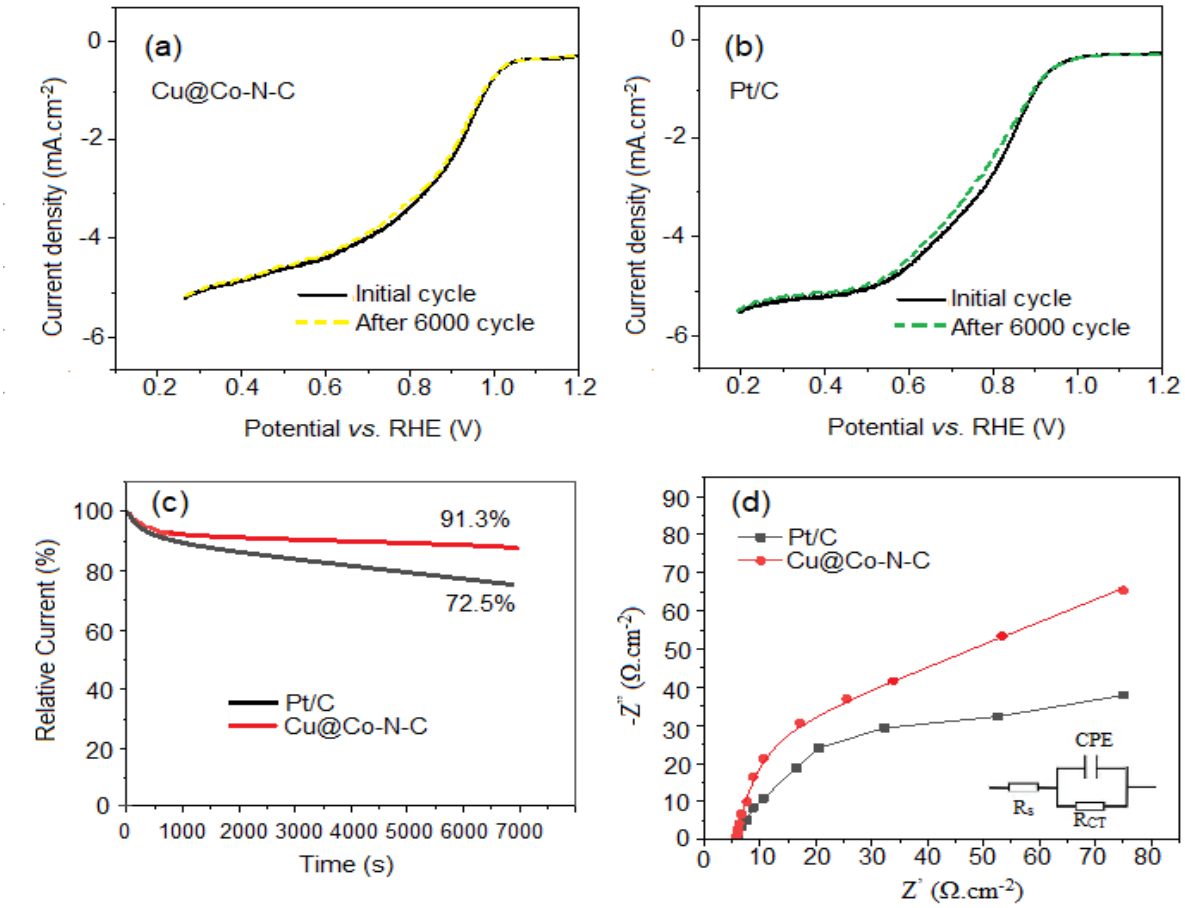

Fig. 4. (a) LSV plots of Cu@Co-N-C, (b) Pt/C for the first and 6000th cycles, (c) Chronoamperometric measurements for Cu@ Co-N-C and Pt/C with a rotation rate of 1600 rpm at 0.75 V for 7000 s, and (d) Electrochemical impedance spectroscopy for Cu@ Co-N-C, and Pt/C electrocatalysts presented in Nyquist plots for the range of 10 KHz-1 mHz in 0.75 V vs. RHE.

excellent ORR activity with a half-wave potential of 0.88 V and superior durability (≈94.6% activity retention after 7000 s) when compared with Pt/C in 0.1 M KOH. This work opens up a new opportunity for rational design and construction of high-performance nonprecious-metal catalysts for energy conversion and storage applications.

Acknowledgment

The authors would like to acknowledge the Hydrogen and Fuel Cell Research Laboratory, Department of Chemistry, Yasouj University.

References

[1] Akbarian P. Kheirmand M. Faraji M. "Facile electrochemical fabrication of high-performance graphene quantum dots-supported Mn3O4/Ag hybrid catalyst for oxygen reduction reaction in alkaline media", Int. J. Energy Res., 2022, 46: 23004.

[2] Amiinu I. S. Pu Z. Liu X. Owusu K. A. Monestel H. G. R. Boakye F. O. Zhang H. Mu S. "Multifunctional Mo–N/C@ MoS2 electrocatalysts for HER, OER, ORR, and Zn–air batteries", Adv. Funct. Mater., 2017, 27: 1.

[3] Girishkumar G. McCloskey B. Luntz A. C. Swan-

son S. Wilcke W. “Lithium-Air Battery: Promise and Challenges”, J. Phys. Chem. Lett., 2010, 1: 2193.

[4] Zhou G. Li M. Li Y. Dong H. Sun D. Liu X. Lin X. Ziqi T. Tang Y. “Regulating the electronic structure of CoP nanosheets by O incorporation for high-efficiency electrochemical overall water splitting”, Adv. Func. Mater., 2020, 30: 1.

[5] Wan X. Liu X. Li Y. Yu R. Zheng L. Yan W. Wang H. Xu M. Shui J. “Fe-N-C electrocatalyst with dense active sites and efficient mass transport for high-performance proton exchange membrane fuel cells”, Nat. Catal., 2019, 2: 259.

[6] Zhang L. Doyle-Davis K. Sun X. “Pt-Based electrocatalysts with high atom utilization efficiency: from nanostructures to single atoms”, Energy Environ. Sci., 2019, 12: 492.

[7] Katsounaros I. Cherevko S. Zeradjanin A. R. Mayrhofer K. J. “Oxygen electrochemistry as a cornerstone for sustainable energy conversion”, Angew. Chem. Int. Ed., 2014, 53: 102.

[8] Zhang K. Zhang Y. Zhang Q. Liang Z. Gu L. Guo W. Zhu B. Guo S. Zou R. “Metal-organic framework-derived Fe/Cu-substituted Co nanoparticles embedded in CNTs-grafted carbon polyhedron for Zn-air batteries”, Carbon Energy, 2020, 2: 283.

[9] Shao M. Chang Q. Dodelet J.-P. Chenitz R. “Recent advances in electrocatalysts for oxygen reduction reaction”, Chem. Rev., 2016, 116: 3594 .

[10] Wang Z. Jin H. Meng T. Lia K. Meng W. Yang J. He D. Xiong Y. Mu S. “Fe, Cu-coordinated ZIF-derived carbon framework for efficient oxygen reduction reaction and zinc–air batteries”, Adv. Func. Mater., 2018, 28: 1.

[11] Meng F. L. Liu K. H. Zhang Y. Shi M. M. Zhang X. B. Yan J. M. Jiang Q. “Recent advances toward the rational design of efficient bifunctional air electrodes for rechargeable Zn–air batteries”, Small, 2018, 14: 1.

[12] Ma X. Li K. Zhang X. Wei B. Yang H. Liu L. Zhang M. Zhang X. Chen Y. “The surface engineering of cobalt carbide spheres through N, B co-doping achieved by room-temperature in situ anchoring effects for active and durable multifunctional electrocatalysts”, J. Mater. Chem. A, 2019, 7: 14904.

[13] Sun M. Davenport D. Liu H. Qu J. Elimelech M. Li J. “Highly efficient and sustainable non-precious-metal Fe–N–C electrocatalysts for the oxygen reduction reaction”, J. Mater. Chem. A, 2017, 6: 2527.

[14] Sun M. Zhang G. Liu H. Liu Y. Li J. “α-and γ-Fe 2 O 3 nanoparticle/nitrogen doped carbon nanotube catalysts for high-performance oxygen reduction reaction”, Sci. China Mater., 2015, 58: 683.

[15] Wu Y. J. Wu X. H. Tu T. X. Zhang P. F. Li J. T. Zhou Y. Huang L. Sun S. G. “Controlled synthesis of FeNx-CoNx dual active sites interfaced with metallic Co nanoparticles as bifunctional oxygen electrocatalysts for rechargeable Zn-air batteries”, Appl. Catal. B: Environ., 2020, 278: 1

[16] Antolini E. “Structural parameters of supported fuel cell catalysts: The effect of particle size, inter-particle distance and metal loading on catalytic activity and fuel cell performance”, Appl. Catal. B-Environ., 2016, 181: 298.

[17] Deng Y. Dong Y. Wang G. Sun K. Shi X. Zheng L. Li X. Liao S. “Well-defined ZIF-derived Fe–N codoped carbon nanoframes as efficient oxygen

reduction catalysts", ACS Appl. Mater. Interfaces, 2017, 9: 9699.

[18] Chung H. T. Cullen D. A. Higgins D. Sneed B. T. Holby E. F. More K. L. Zelenay P. "Direct atomic-level insight into the active sites of a high-performance PGM-free ORR catalyst", Science, 2017, 357: 479.

[19] Jiao L. Seow J. Y. R. Skinner W. S. Wang Z. U. Jiang H. L. "Metalorganic frameworks: structures and functional applications", Mater. Today., 2019, 27: 43.

[20] Wu H. B. Lou X. W. D. "Metal-organic frameworks and their derived materials for electrochemical energy storage and conversion: promises and challenges", Sci Adv., 2017, 3: 1.

[21] Chen Y. Ji S. Wang Y. Dong J. Chen W. Li Z. Shen R. Zheng L. Zhuang Z. Wang D. Li Y. "Isolated single iron atoms anchored on N-doped porous carbon as an efficient electrocatalyst for the oxygen reduction reaction", Angew. Chem., Int. Ed., 2017, 56: 6937.

[22] Nørskov J. Rossmeisl J. Logadottir A. Lindqvist L. "Origin of the overpotential for oxygen reduction at a fuel-cell cathode", J. Phys. Chem. B., 2004, 108: 17886.

[23] Kuang M. Wang Q. Han P. Zheng G. "Cu, Co-embedded N-enriched mesoporous carbon for efficient oxygen reduction and hydrogen evolution reactions", Adv. Energy Mater., 2017, 7: 1.

[24] Morales D. M. Kazakova M. A. Dieckhöfer S. Selyutin A. G. Golubtsov G. V. Schuhmann W. Masa J. "Trimetallic Mn-Fe-Ni oxide nanoparticles supported on multi-walled carbon nanotubes as high-performance bifunctional ORR/OER electrocatalyst in alkaline media", Adv. Func. Mater., 2020, 30: 1.

[25] Sun T. Zhang P. Chen W. Wang K. Fu X. Zheng T. Jiang J. "Single iron atoms coordinated to g-C3N4 on hierarchical porous N-doped carbon polyhedra as a high-performance electrocatalyst for the oxygen reduction reaction", Chem Comm, 2020, 56: 798 .

[26] Wu Y. J. Wu X. H. Tu T. X. Zhang P. F. Li J. T. Zhou Y. Huang L. Sun S. G. "Controlled synthesis of FeNx-CoNx dual active sites interfaced with metallic Co nanoparticles as bifunctional oxygen electrocatalysts for rechargeable Zn-air batteries", Appl. Catal. B, 2020, 278: 1.

[27] Pan Y. Sun K. Liu S. Cao X. Wu K. Cheong W. C. Chen Z. Wang Y. Li Y. Liu Y. Wang D. Peng Q. Chen C. Li Y. "Core–Shell ZIF-8@ZIF-67-Derived CoP Nanoparticle-Embedded N-Doped Carbon Nanotube Hollow Polyhedron for Efficient Overall Water Splitting", J. Am. Chem. Soc. 2017, 140: 2610.

[28] Deng Y. Chi B. Li J. Wang G. Zheng L. Shi X. Cui Z. Du L. Liao S. Zang K. Luo J. Hu Y. Sun X. "Atomic Fe-Doped MOF-Derived Carbon Polyhedrons with High Active-Center Density and Ultra-High Performance toward PEM Fuel Cells", Adv. Energy Mater., 2019, 9: 1.

[29] Akbarian P. Kheirmand M. Asadi A. "Bimetallic 3D hollow-nanoshell FeCo-oxynitride/N and S co-doped carbon nanotubes as a robust bifunctional oxygen electrocatalyst for rechargeable Zn-air batteries", J. Mater. Sci., 2023, 58: 8889.

[30] Qin X. Huang Y. Wang K. Xu T. Wang Y. Wang M. Zhao M. Gao Q. "Highly Efficient Oxygen Reduction Reaction Catalyst Derived from Fe/Ni

Mixed-Metal–Organic Frameworks for Application of Fuel Cell Cathode", Ind. Eng. Chem. Res., 2019, 58:10224.

[31] Wang Y. Zhang B. Pan W. Ma H. Zhang J. "3 D porous nickel–cobalt nitrides supported on nickel foam as efficient electrocatalysts for overall water splitting", ChemSusChem, 2017, 10: 4170.